Nickel Selenide as Efficient Electrocatalyst for Selective Reduction of Carbon Dioxide to Carbon-rich Products

ARTICLE

Nickel Selenide as Efficient Electrocatalyst for Selective Reduction of Carbon Dioxide to Carbon-rich Products

Apurv Saxena[a], Wipula Liyanage[a], Shubhender Kapila[a], Manashi Nath[a]*

Identifying new catalyst composition for carbon dioxide electroreduction to high value products has been at the center of attraction over the last several years. In this article, nickel selenide, $NiSe_2$ has been identified as a high efficiency electrocatalyst for CO_2 electroreduction at neutral pH. Interestingly, $NiSe_2$ shows high selectivity towards specific reduction products forming carbon-rich C2 products like ethanol and acetic acid exclusively at lower applied potential with 98.45% Faradaic efficiency, while C1 products formic acid and carbon monoxide formed preferentially at higher applied potential. More importantly, the C2 products such as acetic acid and ethanol are obtained at very low applied potential, which further corroborates the novelty of this catalyst in CO_2 utilization with minimal energy expense. The $NiSe_2$ catalyst surface has been studied through density functional theory calculations which show that the adsorption energy of intermediate CO on the $NiSe_2$ surface is optimal for extensive reduction through formation of C-C bonds, but not strong enough for surface passivation, thus leading to high selectivity for C2 products. Such high efficiency of the catalyst can be a result of increased covalency of the selenide anion along with high d-electron density of the Ni center. The hydrothermally synthesized $NiSe_2$ sample also shows high activity for oxygen evolution through electrocatalytic water splitting in alkaline medium, effectively making it a bifunctional catalyst which can lower the concentration of atmospheric pollutant CO_2 while at the same time enrich the air with O_2.

Introduction

The continuous consumption of fossil fuels to support today's fast paced economic and social growth has led to serious energy crisis and environmental problems. Atmospheric levels of CO_2 have reached an all-time high of 415 ppm which along with the global warming has also caused several catastrophic consequences including effects on human health, extinction of species leading to ecological imbalance, and food shortage. While researchers are trying to reduce our dependence on fossil fuels by identifying alternative sources of clean energy which will also curb further production of carbon dioxide, there is still a need to reduce the existing vast amount of CO_2 already present. Sequestration and storage can mitigate that problem to a small extent, however, utilization of CO_2 to produce fuels and other valuable chemicals can significantly reduce atmospheric CO_2 levels and close the carbon-cycle loop efficiently. Another imminent necessity is to utilize the copious quantities of CO_2 being produced from various industrial sectors and generate value-added end-products thereby reducing carbon footprint. Carbon dioxide electroreduction (CO2RR) is an effective technique to convert atmospheric CO_2 to valuable products and has been researched widely over the past several decades.[1] Carbon dioxide electroreduction is facilitated by the use of catalysts and the primary challenge is to identify catalyst composition that can convert CO_2 to carbon-rich high-value products with high faradaic efficiency (FE) and high selectivity towards specific products. Among these, product selectivity towards high value products plays a significant role in defining catalyst efficiency as well as practical useability. The high value products of particular importance include formic acid, acetic acid, ethanol, and methanol. As recent research activities have led to discovery of several catalyst compositions, however, optimizing CO2RR while reducing hydrogen evolution reaction from electrocatalytic reduction of water remains a great challenge. Hence, identifying catalysts which can promote CO2RR and suppress the competing HER will be an important step in this field.

Recent research has identified several catalyst compositions for efficient CO2RR. However, among these copper based compositions have showed predominance as effective catalysts leading to a wide range of products.[2–4] Several researchers have reported CO2RR with metallic Cu as well as copper oxide catalysts.[5] Apart from Cu, other metals like Sn and Pb has been also explored as catalysts by different research groups.[6] Similarly, mixed metal alloys such as Cu-Ni and Cu_3Pd have been utilized for CO2RR which have been shown to produce methanol.[6,7] It was observed that Cu hollow fibers when functionalized with Au and Ni enhances reduction of CO_2 to yield CO.[9] Cu(II) and Bi(III)-based MOFs were also found to be

active for CO_2 electroconversion with FE = 28.6 % for C_2H_5OH and FE = 8.6% of CH_3OH.[10] Metal–organic porous materials are also functional for electrochemical conversion of CO_2 to alcohols, promoting low-carbon economy.[11] Cu single atoms dispersed in carbon nanofibers showed enhanced Faradaic efficiency and good partial current density towards methanol after CO2RR.[12] Gas-diffusion electrodes on the other hand, using Cu_2O and Cu_2O–ZnO mixtures leads to high conversion efficiency of CO_2 (54.8% and 31.4% for Cu_2O and Cu_2O/ZnO-based electrodes, respectively) at −1.39 and −1.16 V vs. Ag/AgCl leading to the production of methanol and ethanol.[13] In-Sn alloy catalyst on the other hand, produces formic acid from CO2RR.[14] Nitrogen doped nanodiamonds over silicon rod array have also been proven as efficient electrocatalyst in converting CO_2 to acetic acid with the onset potential of −0.36 V (vs RHE).[15] NiO/MWCNT composite, on the other hand, produces syn gas upon CO2RR.[16] Apart from metals, metallic alloys, and oxides, chalcogenides have also been recently explored as electrocatalysts for CO2RR.[17] Recently Cu_2Se has been identified as efficient CO2RR electrocatalyst with high efficiency.[3,18] Interestingly Cu_2Se shows high selectivity towards carbon-rich products for low applied potentials, with more than 70% Faradaic efficiency for formation of ethanol.[3] Graphene supported NiO/Ni nanoparticles are also explored as efficient photocatalyst for CO_2 reduction with H_2. Under continuous flow, 50 mg of NiO/Ni-G photocatalyst produced CH_4 at rate 244.8 μL h^{−1} with a residence time of 3.1 s.[19]

Catalyst design plays an important role in defining efficiency especially with respect to product selectivity. As we have proposed earlier, formation of carbon-rich products is enhanced by longer dwell time of adsorbed carbon monoxide (*CO) formed as an intermediate on the catalyst surface, which provides more opportunities for further reduction. Another parameter than enhances CO_2 electroreduction is the improved conductivity of the catalyst surfaces which enhances electron transfer especially at lower applied potential which can reduce rate of competing HER. The first parameter can be optimized by selecting transition metal centers that can potentially increase metal-to-ligand back bonding with the intermediate surface-adsorbed CO thereby increasing *CO adsorption energy on the surface. We propose that transition metals with more than half-filled d-orbitals can effectively optimize such back bonding leading to moderate *CO dwell times that will lead to further reduction while not poisoning the catalyst surface. Conductivity and efficient charge transfer on the catalyst surface on the other hand, can be improved by increasing covalency of the lattice anions which leads to decreasing bandgap as has been shown earlier through density functional theory (DFT) studies.[20] We propose that effective application of such catalyst design principles by optimizing charge transfer and intermediate *CO retention on the catalyst surface will lead to efficient CO2RR catalysts that can lead to preferential formation of carbon-rich reduction products with high selectivity at lower applied potentials.

In this article, we have investigated the efficient electroreduction of CO_2 selectively to C1 and C2 products such as formic acid, methanol, ethanol, and acetic acid on hydrothermally synthesized nanoporous $NiSe_2$ electrocatalyst surfaces. High product selectivity could be achieved by varying the applied potential where C1 products formed at higher applied potential while C2 products formed predominantly at lower applied potentials. More importantly, it was observed that the product composition could be made to be exclusively acetic acid by maintaining lower applied potential. Acetic acid is an important industrial chemical[21] and selective production of this through waste CO_2 utilization can be viewed as another novelty of this research. DFT calculations were also performed to estimate the intermediate *CO adsorption energy on the catalyst surface which was observed to be moderately strong suggesting longer *CO dwell time on the catalytic site without poisoning effect. It must be noted here that most of the existing CO2RR catalysts are based on Cu, and Ni-based system has been studied very rarely for CO2RR. This is the first report of Ni-chalcogenides as active catalyst for CO_2 reduction. Moreover, $NiSe_2$ also exhibits formation of carbon-rich products with high Faradaic efficiency at low applied potential which increases novelty of this catalyst system. High product selectivity at low energy expense also makes this $NiSe_2$-based catalyst highly applicable for CO_2 reduction at points of generation as well as stored gas. Previously $NiSe_2$ was explored as a good electrocatalyst for oxygen evolution reaction (OER).[22] Hence this catalyst was applied as bifunctional catalyst that could reduce atmospheric CO_2 to value-added chemicals, and at the same time enrich the atmosphere with O_2 produced through water electrolysis, thereby providing opportunities for environmental remediation.

Materials and Methods:

Synthesis of $NiSe_2$:

Hydrothermal method was used to synthesize $NiSe_2$ following a previously reported procedure.[22] In 15mL deionized water, 10 mmols of $NiCl_2.6H_2O$ and 20 mmols of SeO_2 were mixed by stirring on a magnetic stirrer for 15 minutes. Then 0.2 ml (0.6 mols) of hydrazine monohydrate was added with further stirring for 15 minutes. This solution was then transferred to 23 ml Teflon-lined stainless steel autoclave and heated at 145°C for 24 hours. The autoclave was cooled to room temperature under ambient conditions, and the product was collected through filtration. After washing several times with DI water and ethanol, the solid product was dried overnight in an oven maintained at 35°C.

Preparation of Electrode:

4 mg of the powder $NiSe_2$ was dispersed in 200 μL of 1% Nafion in ethanol. The mixture was sonicated for 30 mins to produce a homogeneous catalyst ink. 20 μL of the catalyst ink was drop casted on to the Carbon Fiber Paper (CFP) at room temperature to prepare the $NiSe_2$-modified electrode. Finally, the as-prepared electrode was allowed to dry at room temperature for 8 hrs. Catalyst loading on the working electrode was calculated to be 1.25 mg cm^{-2} for most of the electrochemical experiments done in this study.

Electrochemical Measurements:

The electrochemical activity of $NiSe_2$ was measured by using a 3-electrode system where $NiSe_2$-modified CFP electrode was used as the working electrode, while Ag|AgCl and glassy carbon

(GC) was used as the reference and counter electrodes, respectively. A H-cell was used for all electrochemical studies where the cathodic and anodic chambers were separated by an anion exchange membrane (Nafion 115). The catholyte and anolyte consisted of 30 ml of 0.3 M $NaHCO_3$ and 1 M KOH, respectively. The Ag|AgCl reference electrode was calibrated with a Pt wire in H_2-saturated H_2SO_4 and an open circuit potential was obtained as −0.199 V. The potential reported vs Ag|AgCl was changed to reversible hydrogen electrode (RHE) using the Eq. (1):

$$E_{RHE} = E_{Ag|AgCl} + 0.059pH + E^0_{Ag|AgCl} \qquad (1)$$

where E_{RHE} is the transformed potential vs RHE. $E_{Ag|AgCl}$ is the experimentally obtained potential. $E^0_{Ag|AgCl}$ is the standard potential of Ag|AgCl (0.199 V). The pH of CO_2 saturated 0.3 M $NaHCO_3$ was estimated to be 6.8.

It must be noted that all electrochemical measurements were performed by following standard protocol as has been reported previously by Clark et al.[23] Accordingly electrochemical carbon dioxide reduction was conducted in stirred solution with rapid bubbling of CO_2 to reduce effect mass transport limitations. Flat carbon fiber substrates with minimal surface roughness were used as working electrodes for similar purpose. We have also calibrated our electrochemical setup by carrying out CO_2 reduction reaction on Ag-modified electrodes which shows similarity with previous reports as has been shown in the following sections.

RESULTS AND DISCUSSION

The composition of the product was confirmed through powder X-ray diffraction (PXRD). As can be seen in the PXRD pattern shown in Figure 1, diffraction peaks from the as synthesized product could be matched with the standard $NiSe_2$ phase (PDF# 01-088-1711) confirming phase purity and crystallinity of the as-synthesized product. Significant broadening of the diffraction peaks was observed suggesting presence of nanostructured grains. Using Scherrer equation, average size of the crystalline domain was estimated to be 27.43 nm.

This stability was confirmed later by doing chronoamperometric stability studies. (Figure S1). We believe that the affinity of nickel to form Ni-CO complex is the driving factor for C2 product formation.

Catalyst morphology was observed through SEM which showed that the hydrothermally frormed $NiSe_2$ formed nanostructured grains as shown in Figures 2a and b, with sizes ranging from 100 – 800 nm and exhibiting considerable surface roughness. The composition of granular nanostructures was confirmed through EDS (Figure 2c) which confirmed the existence of Ni and Se in the film with an approximate ratio of 1:2 and validated the composition as $NiSe_2$. The EDS measurements were usually made on different points of the catalyst surface to confirm uniformity of composition. While EDS confirmed the presence of Ni and Se consistently all through the example, it also affirmed absence of even trace amounts of oxygen, affirming that the sample composition was indeed pure $NiSe_2$. Elemental composition of the hydrothermally synthesized product was further confirmed through X-ray photoelectron spectroscopy

(XPS) measured from pristine surfaces without any sputtering. Calibration was performed using C 1s peak (284.6 eV) and fitting by the Gaussian fitting method.[24] The high-resolution XPS spectra showed peaks corresponding to Ni 2p and Se 3d as shown in Figure 2. The peaks observed at 855.8 and 873.5 eV could be assigned to Ni^{2+} present in $NiSe_2$.[24,25] Se XPS peaks were obtained at binding energies of 55.0 eV and 59.0 eV corresponding to Se $3d_{5/2}$ and Se $3d_{3/2}$ (Figure 2e).[24] It must be noted here that no peaks of Ni- and/or Se-oxide were observed indicating compositional purity of the catalyst surface.

To test electrochemical activity of the catalyst towards CO_2 electroreduction, linear sweep voltammetry (LSV) was performed at a scan rate of 10 mV s^{-1} in Ar- and CO_2-saturated 0.3 M $NaHCO_3$ electrolyte solutions. It was observed that $NiSe_2$@CFP showed higher cathodic current in the polarization curve in CO_2 saturated electrolyte compared to the Ar-saturated electrolyte which proves that CO_2 electroreduction overcomes the competing HER process as can be seen in the Figure 3a. Similar measurements were also performed with blank CFP electrode to study the effect of substrate only, as shown in Figure 3a. Interestingly, it was observed that the cathodic current of blank CFP in CO_2 saturated electrolyte was similar to that in the Ar-saturated electrolyte suggesting that it had no activity towards CO_2 electroreduction under these operational conditions. The LSV studies as shown in Figure 3a further confirms that although CFP (substrate) showed no activity towards CO2RR, the $NiSe_2$ coated CFP substrate has high catalytic activity towards CO2RR exhibiting high current density reaching up to 35 mA.cm^{-2} at low applied potential.

The kinetics of a reaction and electrocatalytic activity, was estimated from the Tafel slope using the Tafel equation as shown in Eq. (2):

$$\eta = \alpha + (2.3RT)\log j/\alpha nF \qquad (2)$$

where η represents the overpotential, n is the number of electrons involved in the reaction, α represents the transfer coefficient, F represents the Faraday constant, j is symbol of the current density and the slope is calculated by $2.3RT/\alpha nF$.

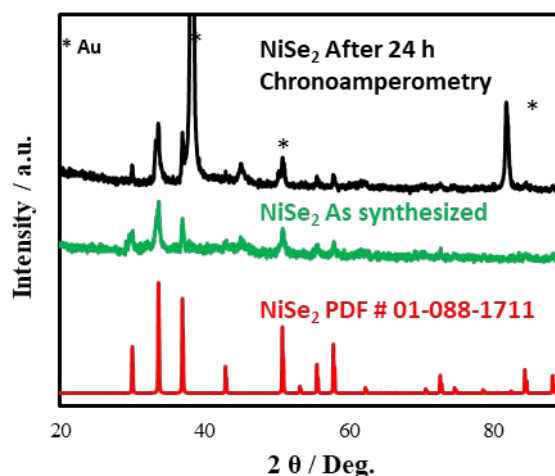Fig 1. PXRD pattern of hydrothermally synthesized $NiSe_2$ compared with the standard $NiSe_2$ reference pattern (PDF # 01-088-1711).

The Tafel equation as represented in Eq. (2) is an important equation which is acquired from the kinetically controlled region of CO2RR and explains the relationship of overpotential η with the current density j. LSV plots were obtained in a non-stirred solution with a slow scan speed (10 mV s^{-1}) for measuring Tafel slopes. The plots were derived from the partial current density and overpotential (the difference in value between the applied potential and the thermodynamic potential). Tafel slope of $NiSe_2$ was estimated to be 129.5 mV dec^{-1} in presence of CO_2 while in absence of CO_2 it showed a much higher Tafel slope. The very low Tafel slope indicates faster kinetics for the reduction of CO_2 in a bicarbonate electrolyte. The Tafel slope for $NiSe_2$ is near to the theoretical value of 118 mV dec^{-1}, which is expected for the chemical rate-determining step (RDS) of initial single-electron transfer step for formation of adsorbed radical intermediate ($CO_2^{\cdot-}$) on the catalyst surface.[26,27] Low Tafel slope values indicating faster intermediate adsorption kinetics at lower applied potential can corroborate well with formation of CO_2 reduction products at lower applied potential including selective formation of carboxylic acids such as acetic acid. The standard reduction potential of CO_2 to acetic acid is 290 mV.[28] The low Tafel slope (129.5 mV dec^{-1}) measured at low overpotential of 290 mV indicates faster kinetics for acetic acid generation illustrating high selectivity and efficiency of the catalyst. However, given the complexity of CO2RR on the catalyst surface and multitude of steps, more studies are needed to correctly ascertain the proper RDS as well as accurate

mechanism for CO2RR on the surface of $NiSe_2$. The Tafel slope for $NiSe_2$@CFP was observed to be smaller than that of bare CFP which confirms the fast transfer of electrons from the $NiSe_2$ modified electrode surface.

To check the product composition formed from CO2RR at $NiSe_2$ modified electrode and evaluate catalyst performance, CO_2 electroreduction studies were performed at different applied potentials (-1.3 V, -1.2 V, -0.9 V, -0.6 V, -0.25 V, -0.1 V vs RHE) in 0.3 M $NaHCO_3$ aqueous solution. The products were collected from the cathodic chamber after 1 h of chronoamperometry at fixed applied potential while the catholyte was subjected to constant purging with CO_2 gas at low flow rate (20 sccm). The liquid-state product identification and quantification were performed through ^1H NMR analysis at different applied potentials. Products in gaseous state were identified and quantified by gas chromatography equipped with thermal conductivity detector (GC-TCD). From NMR plots as shown in Figure 4a, it was observed that the product composition was very dependent on the applied potential and showed selectivity towards specific products at each potential. More interestingly, reduction products generated at low applied potentials were carbon rich compounds like acetic acid and ethanol. It must be noted here that the product composition was exclusively acetic acid for over 150 mV potential range. Acetic acid is an industrially important chemical, and the selectivity towards its production at lower applied potential highlights the novelty of this catalyst. Specifically, this catalyst paves the way for high-
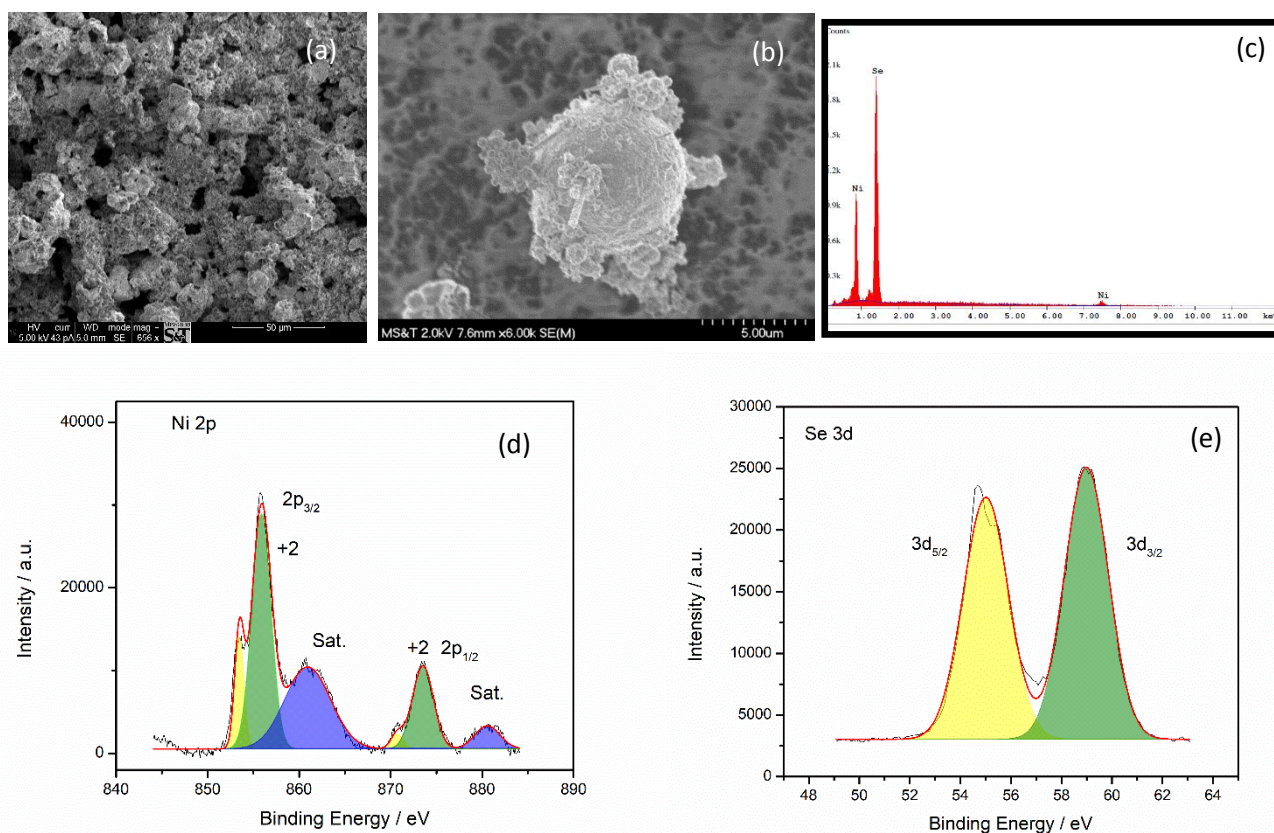

Fig 2. SEM images of the $NiSe_2$ nanoparticles at (a) low and (b) high magnification showing formation of nanostructures and surface roughness, respectively. (c) EDS analysis of the catalyst confirming presence of Ni and Se in 1:2 relative atomic ratio. (d) Ni 2p and (e) Se 3d XPS spectra of as-synthesized $NiSe_2$.
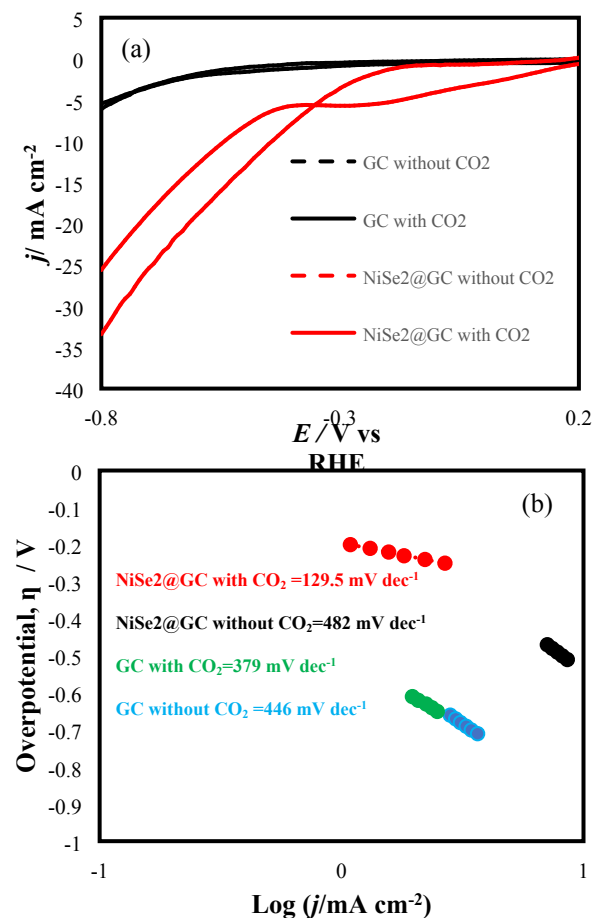
Fig 3. (a) LSVs measured in 0.3 M NaHCO$_3$ at a scan rate of 10 mV s^{-1} in presence and absence of CO$_2$ with NiSe$_2$ modified GC and bare GC electrodes. (b) Tafel plots measured in 0.3 M NaHCO$_3$.

selectivity direct acetic acid synthesis from CO$_2$ replacing the conventional multi-step industrial process which typically begins with synthesis of syngas and ends with the generation of methanol followed by its carbonylation.[29] Moreover, the product composition remained predominantly C2 compounds all the way till -0.6 V vs RHE, which increases novelty of this catalyst even further since most CO2RR catalyst reported previously produces C1 products such as formic acid or CO at similar applied potential. Formation of such carbon-rich products at higher potentials also leads to high production rate due to application of high negative potential. Formic acid was detected in the product composition in addition to carbon rich products at -1.3 V (vs RHE). Hydrogen evolution reaction (HER) occurring at the cathode chamber in aqueous electrolyte is a competitor for CO2RR and has been observed to occur simultaneously. Previous studies has reported that when pH decreases in the vicinity of the electrode surface potential decreases due to continuous hydrogen evolution,[30] in situ conversion of CO$_2$ to HCO$_3^-$ occurs. However, this spontaneous change happens at higher concentration of nascent hydrogen which also leads to formation of formic acid at higher applied potential. The product composition and relative product yield at different applied potentials was quantified using NMR and

the selectivity of C1 and C2 product formation at different applied potentials is shown in Figure 4b. At lower applied potential C2 products (acetic acid and ethanol) are formed exclusively whereas higher applied potentials support the formation of C1 (formic acid) along with some C2 products. This result makes NiSe$_2$ very promising as CO2RR catalyst since for application of any CO$_2$ conversion technology in industrial setup, selectivity is a critical factor. More importantly, the formation of value-added C2 products with less energy expenditure and high selectivity can have practical application in industry. It must be noted here that all electrochemical measurements and product quantification has been done by following standard protocol as described above.[23,31] The electrochemical setup was also calibrated by checking the activity of polycrytalline Ag-modified electrode towards CO$_2$ reduction which shows formation of formic acid and CO at -0.9 V (vs RHE) as has been reported previously,[22] as shown in Figure S2. The current density obatined with Ag-modified electrode was also similar to previous reports as shown in Figure S2.[32,33] A sharp contrast of the product composition was obtained with NiSe$_2$-modified electrodes as shown in Figure S2, confirming the novelty of this electrode.

GC-TCD was used to detect and quantify gaseous products. The head-space gas was collected after 1 h of CO2RR experiment at fixed potential (-0.1 V, -0.25 V, -0.6 V, -0.9 V vs RHE) and was injected into the GC-TCD column. Only H$_2$ was detected as a gaseous product at higher applied potential (> –0.6 V) and no other gaseous product like CO or CH$_4$ commonly observed with previously reported catalysts,[16,19,30,34–42] were detected. Amount of hydrogen gas produced was dependent on the applied potential and increased with increasing cathodic potential (FE = 0 %, 0 %, 0.22%, 0.56 %, 1.27 % at -0.1, -0.25, -0.6, -0.9 and -1.3 V, respectively). HER has been known to be a competing reaction of CO2RR and the challenge is to design catalyst surfaces which can subdue Hydrogen Evolution reaction while reinforcing CO2RR. Hence the observation that even at higher applied potential NiSe$_2$ produces only minor amount of H$_2$, while predominantly forming hydrocarbons, is very promising for electrocatalytic CO2RR. This can be due to the fact that on NiSe$_2$ surface CO$_2$ reduction occurs at much lower applied potential, while HER requires a much higher overpotential as has been reported earlier.[43]

The observed product selectivity also suggests that at lower applied potential intermediate adsorption and kinetics of CO2RR on the catalyst surface is more favorable than rate of water reduction. Moreover, absence of CO in the product composition and production of C2 products selectively, makes NiSe$_2$ catalyst very unique as almost all the nickel-based catalyst are known to produce CO as their main product.[36]

Quantification of gaseous and liquid products was done using combined GC-TCD and NMR measurements, which was further used to calculate individual and total faradaic efficiency (FE) for all the CO$_2$ reduction products that were identified. The Faradaic efficiency for each product was calculated following previously reported standard method[3] where, the electron mole fraction for formation of specific product were considered along with total charge consumed during the electrochemical
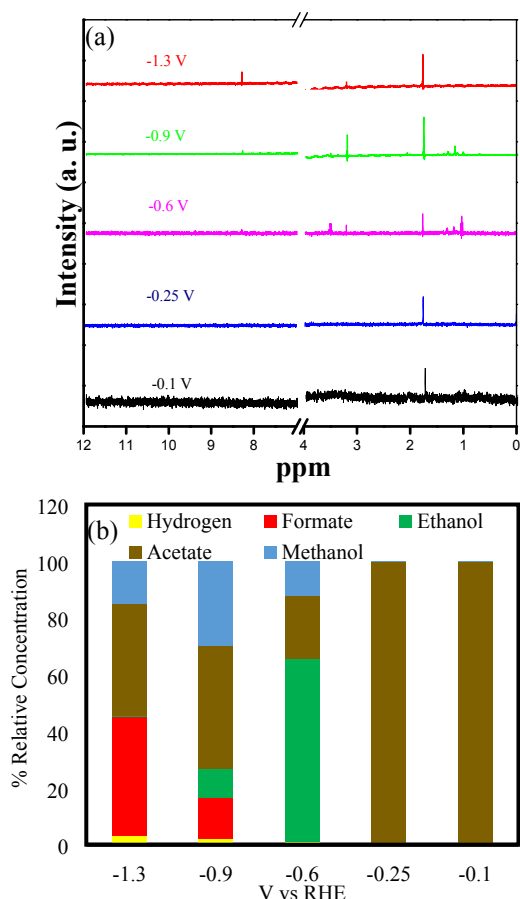
Fig. 4 (a) NMR spectra identifying CO_2 reduction products in reaction aliquots collected at different potentials. (b) Plots illustrating relative concentrations of liquid products and gaseous products quantified from NMR and GC TCD at different reduction potentials.

conversion and mole fractions of products (gaseous and liquid) formed. The absolute quantity of each product was estimated from GC-TCD (gas) and NMR (liquid) experiments. Also, by quantifying the products at any specific potential using GC-TCD and NMR experiments, relative percentage of different products formed was obtained at different potentials.

Faradaic efficiency for all the gaseous as well as liquid products detected using GC-TCD and NMR analysis simultaneously in fixed potential CO2RR experiments has been shown in Figure 5. It was observed that at lower applied potential there was a high selectivity for formation of C2 products such as ethanol and acetic acid as has been explained above from NMR data. Specifically, at the lowest applied potential of 100 mV vs RHE, there was exclusive formation of acetic after 1 h of electrolysis with 97.22% FE. When the applied potential was increased to more negative potential from -0.1 V, new product ethanol was obtained till -0.9 V vs RHE. With the emergence of new products, faradaic efficiency of acetic acid decreased with increasing cathodic potential. Specifically, the Faradaic efficiency for acetic varied from 61.42%, 48.16%, 16.85 %, 98.45 % and 97.22 %, respectively at -1.3, −0.9, −0.6, 0.25, and −0.1 V vs RHE. On the other hand, Faradaic efficiency for ethanol formation varied from 17.59% and 72.14% respectively at−0.9, and -0.6 V vs RHE. Since carbon-rich products such as ethanol

and acetic acid have high industrial value and can also be used as fuels, their exclusive formation at low energy expense can have large implications for practical CO_2 utilization. More importantly, achieving faradaic efficiency of 72.14 % for ethanol at such low applied potential has not been commonly observed in any catalyst systems. Methanol which is a C1 product was first observed at -0.6V reaching its maximum FE at -0.9V. From the figure we can also observe the absence of CO and presence of H_2 in the chromatogram obtained from measurements done on GC-TCD. Alkane products such as methane and ethane were also not observed during the measurement which can be due to: (i) suppression of HER at such low potential as nascent hydrogen produced during HER can be helpful in producing hydrocarbons. (ii) suppression of CO formation which inhibits its further reduction to C1 hydrocarbons such CH_4.

These results show the uniqueness of this electrocatalyst which is able to selectively produce carbon rich fuels with high faradaic efficiency at low energy input. Moreover, this CO2RR electrocatalyst is also capable of producing high current density of 35 mA cm^{-2} at moderately low applied potential.

Stability of the catalyst for CO2RR was checked through chronoamperometry studies where CO_2 was reduced at constant applied potential for 24 hours. The chronoamperometry figures obtained at various applied potentials ranging from -0.1 to -0.9 V vs RHE showed that the reduction current density corresponding to CO2RR was maintained constant for over 12 h as shown in Figure S1 (supporting information). The catalyst composition after CO2RR activity was confirmed through PXRD measurements which showed that there was no change in the crystallinity or composition of the catalyst before and after CO2RR activity (Figure 1).

Phase stability of $NiSe_2$ under operational conditions for CO2RR can be also explained through Pourbaix diagrams which are electrochemical phase diagrams as a function of pH depicting compositional stability of metal and its compounds in the aqueous phase. These phase maps help in assessing the
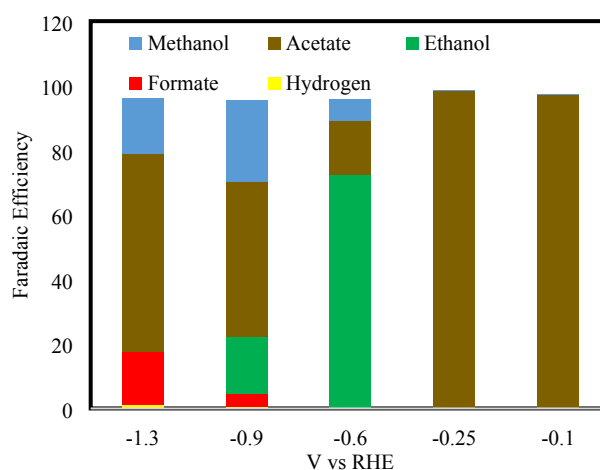

Fig 5. Bar plots depicting relative faradaic efficiency of cumulative liquid and gas phase CO_2 reduction products at different applied potentials quantified through NMR and GC-TCD.
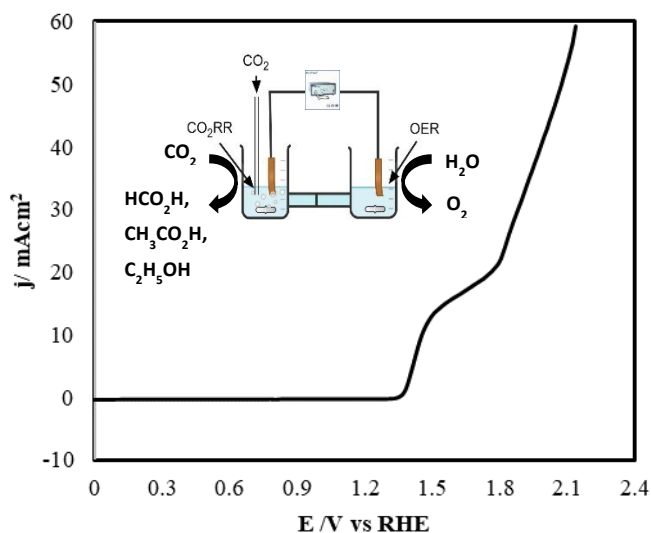
Fig. 6. Polarization curve with cathodic CO2RR and anodic OER with NiSe$_2$@CFP as both cathodic and anodic electrocatalyst. Inset shows schematic of the electrochemical setup for combined CO2RR and OER.

electrochemical stabilities of NiSe$_2$ under various applied potential. Ni Pourbaix diagrams calculated from density-functional theory (DFT) makes $\Delta_f G$ values (free energy of formation) more consistent with direct electrochemical experiments. It was reported previously that the Ni metallic phase forms below -0.75 V vs RHE in the Pourbaix diagram[44] making NiSe$_2$ very stable catalyst on the applied potential range for CO2RR. Specifically, the conversion of Nickel (II) to Nickel (0) requires excess energy/potential in operational pH for CO2RR (i.e., pH = 7.2–8.9).[44] The corrosion rate for Ni^{2+} was also observed to be minimal at neutral pH below 1 V vs RHE. Hence, from the Pourbaix digram it can be confirmed that there is minimal catalyst reduction and degradation at neutral pH under operational condition for CO2RR, illustrating fuinctional and compositional stability of NiSe$_2$. The preferential reduction that occurs on the surface of NiSe$_2$ under these operational conditions is analyte reduction, i.e. CO2RR and HER.

Electrochemical catalytic activity of NiSe$_2$ for CO2RR-OER

It must be mentioned here that NiSe$_2$ has been previously reported as a promising catalyst in alkaline medium for oxygen evolution reaction (OER) [22,35] with an onset potential of 1.36 V (vs RHE) and overpotential of 290 mV at 10 mA.cm^{-2}. Hence, the application of NiSe$_2$ was applied as a bifunctional OER-CO2RR catalyst wherein, the NiSe$_2$@CFP was used both as cathodic catalyst to electrochemically reduce CO$_2$ in the cathodic chamber and also as anodic catalyst for generation of oxygen through water splitting in the anodic chamber. This experiment was done in a H-shaped electrochemical cell where the cathodic and anodic chambers were separated by Nafion membrane. The catholyte was 0.3 M NaHCO$_3$ solution where CO$_2$ was continuously purged while the anolyte consisted of 1 M KOH. The pH of both the chambers were continuously monitored to confirm that there was no transport of OH$^-$ remains across the membrane and catholyte and anolyte maintained their neutral and alkaline nature, respectively. Figure 6 shows the polarization curve obtained for such CO2RR-OER experiment

while a schematic representation of the experimental setup has been shown as an inset in the figure. It was observed that the CO2RR-OER electrolytic cell exhibited a cell potential of ~1.8 V at 20 mA.cm^{-2} indicating high efficiency of the process. The catholyte composition detected through NMR showed presence of ethanol and acetic acid similar to that as has been shown in Figure 4, confirming the occurrence of CO2RR similar to the constant potential experiment. Such bifunctional activity emphasizes the novelty of this catalyst since it can not only reduce the concentration of atmospheric pollutant CO$_2$, but also enrich the air with O$_2$. This will have tremendous impact in practical applicability of such catalysts especially in situations where there is a high concentration of CO$_2$ and access to clean oxygen is needed on-demand.

Enhanced electrocatalytic activity can typically be assigned to intrinsic factors which includes facile catalyst activation through intermediate adsorption and enhanced charge transport, as well as extrinsic factors such as catalyst morphology and surface roughness which influences electrolyte and analyte access to the catalytically active sites. The extrinsic factors affecting CO2RR electrocatalytic activity of NiSe$_2$ was investigated by estimating the electrochemically active surface area (ECSA) by following previously reported experimental procedure.[45,46] The ECSA was calculated by plotting electrochemical double layer capacitance in the non-Faradaic region as a function of scan rate and then comparing specific capacitance (C_S) to the double layer capacitance observed. The electrochemical double layer capacitance (C_{DL}) was calculated following Eq. (3).

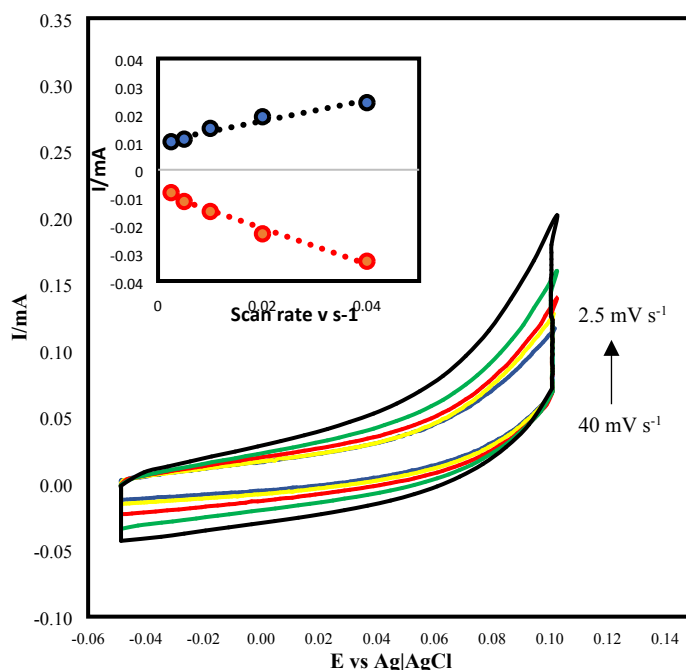$$i_{DL} = C_{DL} \times v \qquad (3)$$

Fig. 7. Cyclic voltammograms measured for NiSe$_2$ catalyst in 0.3 M NaHCO$_3$ under continuous N$_2$ purging at different scan rates from 2.5 to 40 mV s^{-1}. Inset shows plot of anodic and cathodic current measured at 0.04 V vs Ag|AgCl as function of scan rate.

where i_{DL} represents the current observed while v is the scan rate. As can be seen from the Figure 7, C_{DL} calculated from the i vs v plot resulted in value of 0.5 mF.

The ratio of C_{DL} and Cs was used to calculate ECSA as shown in Eq. (4).

$$ECSA = C_{DL}/Cs \quad ---(4)$$

Using the Cs value (40μF cm^{-2}) from reported values and C_{DL} value (0.5 mF) from the plot, ECSA value was calculated to be 12.74 cm^2. The effect of catalyst morphology on the working electrode was also estimated from the roughness factor (RF). RF was calculated to be 159.28 from the ratio between ECSA and geometric electrode area (0.08 cm^2). High value of ECSA and roughness factor depicts that CO_2 dissolved in the electrolyte has more access to the catalytic sites on working electrode, leading to better conversion efficiency. For getting better insights about the selectivity for the CO_2 reduction reaction and to understand reaction kinetics, we analyzed the formation rates and the partial current density (proportional to TOF) for each product over a range of potentials as shown in Figure 8. Such TOF related analysis for different products can lead to crucial information about mechanism. From the plots of reaction rates and partial current density it was observed that acetic acid was the major contributor for enhanced activity over a range of potential. At higher applied potential, formic acid showed comparable formation rate as acetic acid. However, at low applied potential acetic acid and ethanol showed much higher formation rates. It was also observed that acetic acid showed the highest current density at higher applied potential, while partial current density for ethanol increased for lower applied potential. Such activity trends confirmed the product selectivity and novelty of this catalyst compared to other reported CO2RR catalyst which shows higher formation constants for mostly C1 products. Such difference in electrochemical activity can be deduced because of different rate of *CO conversion on the surface as described below. Additionally, the reaction intermediates can also undergo dehydroxylation and decarbonylation with variable rates at different applied potential. These analyses also confirms that $NiSe_2$ is capable of catalyzing the reduction of CO_2 and yielding significant amounts of hydrocarbons with high reaction rates over sustained periods of time.
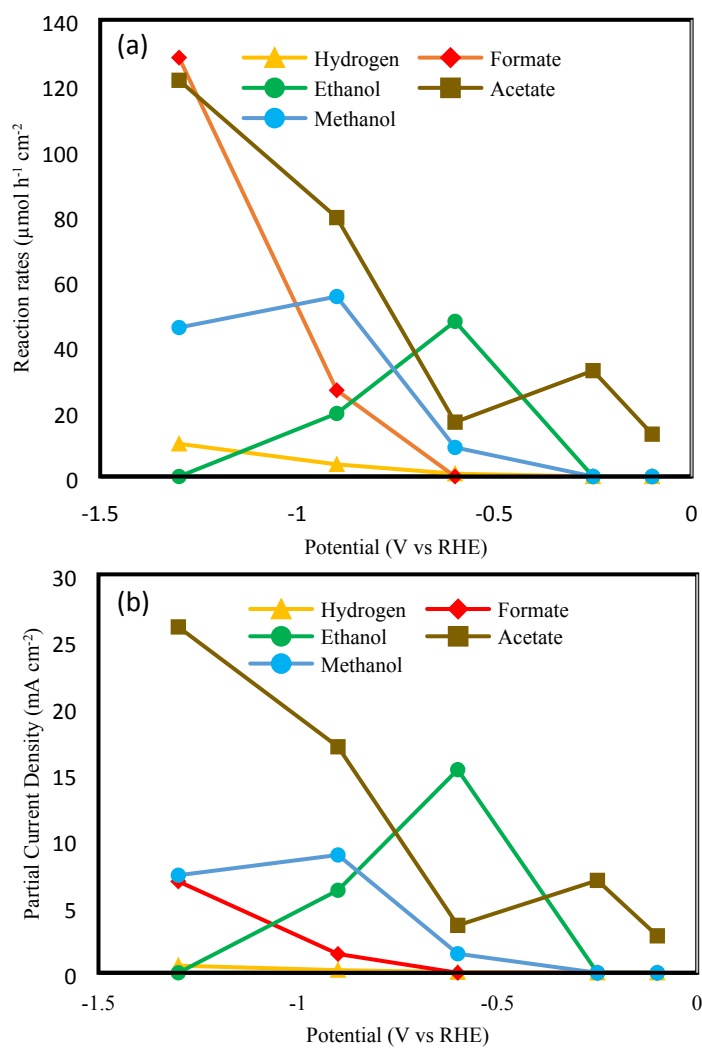
ARTICLE

Fig. 10. CO adsorption energy on $NiSe_2$ (111) surface compared with other known CO2RR reduction catalysts. All CO adsorption energies were estimated through DFT calculations.

catalyst composite. It is imperative that lower R_{CT} values will lead to faster charge transfer rate at the interface resulting in facile reduction on the electrode surface. The R_{CT} and R_s estimated at different potentials has been listed in Table 1. It can be clearly seen that the charge-transfer resistance decreases as a function of applied potential explaining how the reduction current density and efficiency increases with potential. Typically, at higher (applied) negative potentials, the reaction rate increases leading to higher current density. Hence, charge transfer within the catalyst composite as well as at the electrode-electrolyte interface increases leading to decreased R_s and R_{CT} values, respectively.

Fig. 8. CO$_2$RR performances of NiSe$_2$ catalyst. (a) Formation rates of Hydrogen, formate, ethanol, acetate and methanol. (b) Partial current density of individual products, hydrogen, formate, ethanol, acetate and methanol.

The intrinsic effect of catalyst composite on CO2RR activity was investigated through electrochemical impedance spectroscopy (EIS) to investigate the kinetics of charge transfer on NiSe$_2$ catalytic surface during the CO2RR process. Nyquist plots were measured at different potentials ranging from 0 to -1.3 V in CO$_2$-saturated 0.3 M NaHCO$_3$ to investigate how the charge transfer kinetics varied as a function of applied potential and stages of CO$_2$ reduction. These plots also indicate how intermediate adsorption on the catalyst surface may affect the charge transfer kinetics leading to variation in reduction current density and CO2RR efficiency. For instance, at cathode, adsorption of intermediates on catalyst surface can be affected by hydrated Na$^+$ ions which also functions as buffer in solution. In the proximity of cathode, columbic interactions can also cause the hydrolysis of hydrated Na$^+$ cations. The Nyquist plots were fitted to equivalent circuits as shown in inset of Figure 9, in which charge transfer resistance (R$_{CT}$) refers to the electrode-electrolyte interface and illustrates the barrier that electrons must cross to reach the electroactive species adsorbed on the electrode surface, while R$_s$ represents film resistance of the
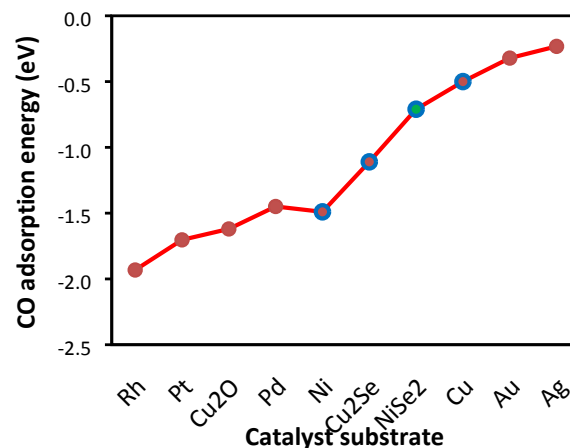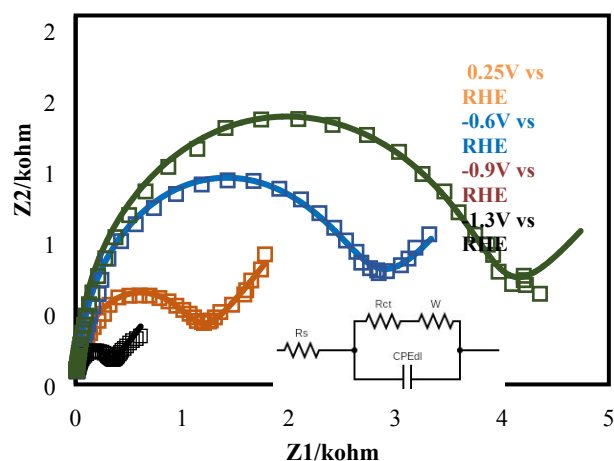

Fig. 9. EIS Nyquist plots of NiSe$_2$@CFP in CO$_2$-saturated 0.3 M NaHCO$_3$ electrolyte (pH 6.8) from 0 V vs RHE to -1.3 V vs RHE. Inset shows the equivalent circuit fitted to experimental spectra, where R$_{CT}$ corresponds to the charge-transfer resistance on catalyst-electrolyte interface, while R$_s$ indicates film resistance of the catalyst composite.

Table 1: Fitting parameters obtained from Nyquist plots at various potentials.

Potential (V vs RHE)	Rct	Rs	CPE$_{dl}$	W
-0.25	36.78	17.8	0.50	0.0000915
-0.6	25.07	3.77	0.91	0.00011
-0.9	10.23	3.6	1.14	0.00012
-1.3	2.80	2.6	1.3	0.00029

Large ECSA ensures better electrolyte access to catalytically active sites while low charge transfer resistance and film resistance facilitates charge transfer across the electrode-electrolyte interface and within the catalyst matrix. Both of these factors can enhance the reduction current density while lowering the potential required for CO2RR. Another factor that can influence such electrocatalytic activity is the catalyst surface wetting with aqueous electrolyte which maximizes electrolyte access on the surface and enhances intermediate adsorption. Surface wetting can be qualitatively estimated through measuring contact angle of the electrolyte drop on the catalyst-electrode surface. Difference in the contact angle of the electrolyte with NiSe$_2$@CFP and CFP was observed as shown in Figure S3. Increased contact angle in NiSe$_2$@CFP indicates better hydrophilicity and surface wetting which increases the exposure of active sites in catalyst for CO$_2$ electroreduction. [47]

The product selectivity and composition on the other hand, depends heavily on the nature and energetics of intermediate adsorption on the catalyst surface. Previously we have proposed that carbon monoxide (*CO) formed through initial reduction of the anion radical CO$_2$·$^−$ on catalyst surface plays a significant role as the reactive intermediate. The dwell time of *CO on the catalyst surface is proposed to influence the extent of CO$_2$ reduction and product composition. A longer dwell time of intermediate *CO will expectedly lead to further reduction of CO$_2$ to carbon rich (C2 and C3) products, while lesser dwell time will lead to ready release of CO or formic acid as the reduction products(s). The *CO dwell time on the surface can be inferred from the *CO adsorption energy on the surface. The *CO adsorption energy on NiSe$_2$ surface was calculated through density functional theory (DFT) approach following methodology as described previously.[3] Details of DFT calculations has been provided in supporting information. It was observed that *CO adsorption energy on NiSe$_2$ surface was smaller than that of Ni metal, but higher than that of Cu. Earlier we had proposed that the *CO adsorption energy could be directly correlated to the observed product selectivity with smaller *CO adsorption energy leading to C1 products (CO and formic acid), while higher adsorption energy leads to catalyst poisoning. This hypothesis was based on the plot shown in Figure 10 and comparison with reported literature from various groups. Catalysts such as Au, Ag, and Cu with very low CO adsorption energy traditionally produces CO and formic acid from CO$_2$, while Pt, Pd, Ru etc. are easily poisoned by CO$_2$. In Cu-based system it was shown that intermediate *CO adsorption energy led to preferential formation of C2 products in Cu$_2$Se.[3] Hence, we had proposed the mid-section of this plot represents optimal *CO adsorption energy which maximizes CO dwell time

for subsequent reduction to carbon-rich products without leading to catalyst poisoning. It was observed that CO adsorption energy of NiSe$_2$ is indeed in the middle region illustrating optimal catalyst composition for CO$_2$ reduction to C2/C3 products. It must also be noted that the CO adsorption energy on NiSe$_2$ surface was lower than that of Ni. This can be attributed to the fact that CO adsorption on transition metal site is influenced by the possibility of forming metal-ligand back bonding involving metal d-orbitals and π* orbitals of CO. Such overlap will be affected by the proximity of the d- and π* orbitals. In this case, as oxidation state of the metal site increases in NiSe$_2$ (Ni^{2+}), the d-orbital energies become more stabilized leading to a lesser degree of overlap compared to metal in 0 oxidation state (Ni). Hence, it can be expected that the metal-to-ligand back bonding in metallic Ni is stronger than that in NiSe$_2$ due to better overlap attributed to closer proximity of the participant orbitals. It should also be noted that this observation is in sharp contrast with Cu and Cu$_2$Se where Cu has smaller *CO adsorption energy compared to Cu$_2$Se. This difference can be attributed to the d^{10} full shell configuration of Cu which imparts extra stability leading to large separation between the d- π* orbitals. Hence, it becomes important to realize the importance of d-shell occupancy on the extent of metal-to-ligand back bonding and its effect on the CO2RR outcome. Electronegativity of the anion also has a critical role to play in metal-to-ligand back bonding, wherein, reducing electronegativity is expected to raise energy of the bonding molecular orbitals leading to smaller gap between the metal and ligand group orbitals. This case study with NiSe$_2$ reveals the importance to understand the effect of such intrinsic factors on the CO2RR activity through its effect on metal-to-ligand back bonding that optimizes intermediate *CO adsorption on the surface and further CO2RR activity.

Conclusions

In summary, NiSe$_2$ was identified as a highly efficient electrocatalyst for CO$_2$ reduction. The NiSe$_2$ was synthesized through one-pot hydrothermal synthesis method. The novelty of this catalyst lies in the fact that it can lead to preferential formation of value-added C2 products at very low applied potential with minimum energy expense. Acetic acid was formed exclusively between a potential range of 100 to 250 mV vs RHE while at slightly higher potential it showed acetic acid and ethanol as the only products after several hours of CO$_2$ reduction. Preferential formation of C1 products such as methanol and formic acid was observed at higher applied potential. Interestingly this catalyst showed negligible presence of CO in the reduction products, thereby isolating it from most of the CO2RR catalysts that has been reported till date. A comparative study of NiSe$_2$ with various reported CO2RR catalysts with respect to product composition has been shown in Figure S4 in supporting information. This comparison further confirms the novelty and uniqueness of the NiSe$_2$ catalyst reported in this manuscript, as it can be clearly seen that while majority of other CO2RR catalysts produces formic acid and CO, NiSe$_2$ preferentially forms acetic acid, ethanol and methanol

with high selectivity and Faradaic efficiency. While benchmarking different catalyst compositions is indeed important, the field of catalysis also progresses through discovery of new/improved catalyst compositions that can go beyond what has already been reported. This is especially true for CO2RR, where majority of the catalyst compositions report CO and HCO_2H (formic acid) as primary products. The $NiSe_2$ catalyst reported in this manuscript thus provides a significant advancement for the field, since it can readily produce high-value products such as acetic acid and ethanol with high selectivity. It should be also noted that formation of H_2 through HER was observed at much higher potential indicating that at low applied potential CO2RR was more kinetically favored on $NiSe_2$ surface. Low R_{CT} between the catalysts and the substrate in the electrodes, moderate binding energy of intermediates on the $NiSe_2$ catalyst and abundant exposed active sites in the nanoporous catalyst composite enhance the efficiency of $NiSe_2$ for reduction of CO_2 to C_2 products. According to applied potential, reduction products of CO2RR showed selectivity between C1 and C2 products. At high applied potential (-1.3 V), formic acid was detected along with acetic acid and methanol with a Faradaic efficiency of 16.23%, 61.42% and 17.32% respectively. At higher anodic potential (<-1.3 V) increased selectivity towards C2 products such as ethanol and acetic acid were obtained. For ethanol, maximum faradaic efficiency was achieved at a low applied potential of -0.6 V vs RHE. Through literature search, it was realized that that these applied potentials are among the lowest applied potential at which C2 products have been obtained with high yield and Faradaic efficiency. The liquid and gaseous reduction products were characterized through NMR and GC-TCD techniques, respectively using time-dependent measurements. H_2 was detected at high cathodic potential (> -0.6 V) reaching its maximum at -1.3 V indicating that $NiSe_2$ has suppressed HER catalytic activity at low overpotentials. Since HER at cathode is a competing reaction and inhibits CO2RR on the catalyst surface, result mentioned above are significant for practical application of this catalyst. Interestingly, there was no CO formed among the reduction products which is different from other catalyst having CO as their major products. The $Nise_2$ catalyst was further studied for the CO_2 electroreduction by estimating CO adsorption energy on the catalyst site using DFT calculations. Calculations showed moderate CO adsorption energies which indicates adsorbed *CO has longer dwell time on the catalyst surface causing selective reduction to C2 products. In summary, $NiSe_2$ catalyst can reduce CO_2 to methanol, ethanol and acetic acid at lowest applied potentials reported till date with high Faradaic efficiency. These experimental results along with the findings of catalytic activity with CO adsorption energy obtained using DFT study can lead to optimal catalyst design for synthesizing carbon-rich high-value products through CO_2 reduction.

Authors Contribution

AS executed all synthesis, characterization, and electrochemical measurements, interpreted and analysed data and prepared initial manuscript draft; W. P. R. L. performed the DFT calculations; S. K. helped with GC-MS measurements; and MN conceptualized the project, obtained financial support, designed course of study and finalized the manuscript draft.

Conflicts of interest

There are no conflicts to declare.

Acknowledgements

References

1   Y. Hori, K. Kikuchi and S. Suzuki, PRODUCTION OF CO AND CH 4 IN ELECTROCHEMICAL REDUCTION OF CO 2 AT METAL ELECTRODES IN AQUEOUS HYDROGENCARBONATE SOLUTION , *Chem. Lett.*, 1985, **14**, 1695–1698.

2   Y. Zheng, A. Vasileff, X. Zhou, Y. Jiao, M. Jaroniec and S.-Z. Qiao, Understanding the Roadmap for Electrochemical Reduction of CO2 to Multi-Carbon Oxygenates and Hydrocarbons on Copper-Based Catalysts, *J. Am. Chem. Soc.*, 2019, **141**, 7646–7659.

3   A. Saxena, W. Liyanage, J. Masud, S. Kapila and M. Nath, Selective Electroreduction of CO2 to Carbon-rich Products by Simple Binary Copper Selenide Electrocatalyst, *J. Mater. Chem. A*, 2021, **9**, 7150–7161.

4   M. Nath, H. Singh and A. Saxena, Progress of Transition Metal Chalcogenides as Efficient Electrocatalysts for Energy Conversion, *Curr. Opin. Electrochem.*, 2022, 100993.

5   K. P. Kuhl, E. R. Cave, D. N. Abram and T. F. Jaramillo, New insights into the electrochemical reduction of carbon dioxide on metallic copper surfaces, *Energy Environ. Sci.*, , DOI:10.1039/c2ee21234j.

6   Z. Yang, F. E. Oropeza and K. H. L. Zhang, P-block metal-based (Sn, In, Bi, Pb) electrocatalysts for selective reduction of CO2to formate, *APL Mater.*, 2020, **8**, 60901.

7   S. Ma, M. Sadakiyo, M. Heim, R. Luo, R. T. Haasch, J. I. Gold, M. Yamauchi and P. J. A. Kenis, Electroreduction of carbon dioxide to hydrocarbons using bimetallic Cu-Pd catalysts with different mixing patterns, *J. Am. Chem. Soc.*, 2017, **139**, 47–50.

8   T. Adit Maark and B. R. K. Nanda, CO and CO2 Electrochemical Reduction to Methane on Cu, Ni, and Cu3Ni (211) Surfaces, *J. Phys. Chem. C*, 2016, **120**, 8781–8789.

9   I. Merino-Garcia, J. Albo, P. Krzywda, G. Mul and A. Irabien, Bimetallic Cu-based hollow fibre electrodes for CO2 electroreduction, *Catal. Today*, 2020, **346**, 34–39.

10   J. Albo, M. Perfecto-Irigaray, G. Beobide and A. Irabien, Cu/Bi metal-organic framework-based systems for an enhanced electrochemical transformation of CO2 to

alcohols, *J. CO2 Util.*, 2019, **33**, 157–165.

11   J. Albo, D. Vallejo, G. Beobide, O. Castillo, P. Castaño and A. Irabien, Copper-Based Metal–Organic Porous Materials for CO2 Electrocatalytic Reduction to Alcohols, *ChemSusChem*, 2017, **10**, 1100–1109.

12   H. Yang, Y. Wu, G. Li, Q. Lin, Q. Hu, Q. Zhang, J. Liu and C. He, Scalable Production of Efficient Single-Atom Copper Decorated Carbon Membranes for CO2 Electroreduction to Methanol, *J. Am. Chem. Soc.*, 2019, **141**, 12717–12723.

13   J. Albo and A. Irabien, Cu2O-loaded gas diffusion electrodes for the continuous electrochemical reduction of CO2 to methanol, *J. Catal.*, 2016, **343**, 232–239.

14   F. Cheng, X. Zhang, K. Mu, X. Ma, M. Jiao, Z. Wang, P. Limpachanangkul, B. Chalermsinsuwan, Y. Gao, Y. Li, Z. Chen and L. Liu, Recent Progress of Sn-Based Derivative Catalysts for Electrochemical Reduction of CO2, *Energy Technol.*, 2021, **9**, 2000799.

15   Y. Liu, S. Chen, X. Quan and H. Yu, Efficient Electrochemical Reduction of Carbon Dioxide to Acetate on Nitrogen-Doped Nanodiamond, *J. Am. Chem. Soc.*, 2015, **137**, 11631–11636.

16   S. M. Bashir, S. S. Hossain, S. ur Rahman, S. Ahmed and M. M. Hossain, NiO/MWCNT Catalysts for Electrochemical Reduction of CO2, *Electrocatalysis*, 2015, **6**, 544–553.

17   X. Shao, X. Zhang, Y. Liu, J. Qiao, X.-D. Zhou, N. Xu, J. L. Malcombe, J. Yi and J. Zhang, Metal chalcogenide-associated catalysts enabling CO2 electroreduction to produce low-carbon fuels for energy storage and emission reduction: catalyst structure, morphology, performance, and mechanism, *J. Mater. Chem. A*, 2021, **9**, 2526–2559.

18   D. Yang, Q. Zhu, C. Chen, H. Liu, Z. Liu, Z. Zhao, X. Zhang, S. Liu and B. Han, Selective electroreduction of carbon dioxide to methanol on copper selenide nanocatalysts, *Nat. Commun. 2019 101*, 2019, **10**, 1–9.

19   D. Mateo, J. Albero and H. García, Graphene supported NiO/Ni nanoparticles as efficient photocatalyst for gas phase CO2 reduction with hydrogen, *Appl. Catal. B Environ.*, 2018, **224**, 563–571.

20   H. Singh, J. Bernabe, J. Chern and M. Nath, Copper selenide as multifunctional non-enzymatic glucose and dopamine sensor, *J. Mater. Res. 2021 367*, 2021, **36**, 1413–1424.

21   F. N. Harris, Applications of Acetic Acid to Well Completion, Stimulation and Reconditioning, *J. Pet. Technol.*, 1961, **13**, 637–639.

22   A. T. Swesi, J. Masud, W. P. R. Liyanage, S. Umapathi, E. Bohannan, J. Medvedeva and M. Nath, Textured NiSe2 Film: Bifunctional Electrocatalyst for Full Water Splitting at Remarkably Low Overpotential with High Energy Efficiency /639/638/77/886 /639/301/299/886 /639/301/299/161 /128 /120 /145 /140/146 article, *Sci. Rep.*, 2017, **7**, 1–11.

23   E. L. Clark, J. Resasco, A. Landers, J. Lin, L. T. Chung, A. Walton, C. Hahn, T. F. Jaramillo and A. T. Bell, Standards and Protocols for Data Acquisition and Reporting for Studies of the Electrochemical Reduction of Carbon Dioxide, *ACS Catal.*, 2018, **8**, 6560–6570.

24   Q. Jiang, R. Chen, H. Chen, J. Jiang, X. Yang, Y. Ju, R. Ji and Y. Zhang, Improved performance in dye-sensitized solar cells via controlling crystalline structure of nickel selenide, *J. Mater. Sci.*, 2018, **53**, 7672–7682.

25   H. van der Heide, R. Hemmel, C. F. van Bruggen and C. Haas, X-ray photoelectron spectra of 3d transition metal pyrites, *J. Solid State Chem.*, 1980, **33**, 17–25.

26   Y. Zhao, J. Liang, C. Wang, J. Ma and G. G. Wallace, Tunable and Efficient Tin Modified Nitrogen-Doped Carbon Nanofibers for Electrochemical Reduction of Aqueous Carbon Dioxide, *Adv. Energy Mater.*, 2018, **8**, 1702524.

27   Y. Hori, in *Modern ASpects of Electrochemistry no 42*, 2008.

28   M. Dworkin, S. Falkow, E. Rosenberg, K.-H. Schleifer and E. Stackebrandt, Eds., The Prokaryotes, , DOI:10.1007/0-387-30742-7.

29   The Cativa™ Process for the Manufacture of Acetic Acid | Johnson Matthey Technology Review, https://www.technology.matthey.com/article/44/3/94-105/, (accessed 18 November 2021).

30   D. Tan, C. Cui, J. Shi, Z. Luo, B. Zhang, X. Tan, B. Han, L. Zheng, J. Zhang and J. Zhang, Nitrogen-carbon layer coated nickel nanoparticles for efficient electrocatalytic reduction of carbon dioxide, *Nano Res.*, 2019, **12**, 1167–1172.

31   K. P. Kuhl, E. R. Cave, D. N. Abram and T. F. Jaramillo, New insights into the electrochemical reduction of carbon dioxide on metallic copper surfaces, *Energy Environ. Sci.*, 2012, **5**, 7050–7059.

32   W. Qiu, R. Liang, Y. Luo, G. Cui, J. Qiu and X. Sun, A Br– anion adsorbed porous Ag nanowire film: in situ electrochemical preparation and application toward efficient CO2 electroreduction to CO with high selectivity, *Inorg. Chem. Front.*, 2018, **5**, 2238–2241.

33   Y. Yu, N. Zhong, J. Fang, S. Tang, X. Ye, Z. He and S. Song, Comparative Study between Pristine Ag and Ag Foam for Electrochemical Synthesis of Syngas with Carbon Dioxide and Water, *Catal. 2019, Vol. 9, Page 57*, 2019, **9**, 57.

34   W. Zheng, C. Guo, J. Yang, F. He, B. Yang, Z. Li, L. Lei, J. Xiao, G. Wu and Y. Hou, Highly active metallic nickel sites confined in N-doped carbon nanotubes toward significantly enhanced activity of CO2 electroreduction, *Carbon N. Y.*, 2019, **150**, 52–59.

35   J. Zhou, L. Yuan, J. Wang, L. Song, Y. You, R. Zhou, J. Zhang and J. Xu, Combinational modulations of NiSe2 nanodendrites by phase engineering and iron-doping towards an efficient oxygen evolution reaction, *J. Mater. Chem. A*, 2020, **8**, 8113–8120.

36   H. Yang, Q. Lin, Q. Zhang, X. Yu, Z. Cheng, G. Li, Q. Hu, X. Ren, Q. Zhang, J. Liu and C. He, Carbon dioxide electroreduction on single-atom nickel decorated carbon membranes with industry compatible current densities, *Nat. Commun.*, 2020, **11**, 1–8.

37   T. Zhang, T. Lin, L. Z. Li, X. He, S. Xiao, V. N. Shanov and J. Wu, Nickel-Nitrogen-Carbon Molecular Catalysts for High Rate CO2 Electro-reduction to CO: On the Role of Carbon Substrate and Reaction Chemistry, *ACS Appl. Energy Mater.*, 2020, **3**, 1617–1626.

38   Z. Wang, P. Hou, Y. Wang, X. Xiang and P. Kang, Acidic Electrochemical Reduction of CO2 Using Nickel Nitride on Multiwalled Carbon Nanotube as Selective Catalyst, *ACS*

Sustain. Chem. Eng., 2019, **7**, 6106–6112.

39   H. Y. Jeong, M. Balamurugan, V. S. K. Choutipalli, E. S. Jeong, V. Subramanian, U. Sim and K. T. Nam, Achieving highly efficient CO2 to CO electroreduction exceeding 300 mA cm-2 with single-atom nickel electrocatalysts, *J. Mater. Chem. A*, 2019, **7**, 10651–10661.

40   C. Yan, H. Li, Y. Ye, H. Wu, F. Cai, R. Si, J. Xiao, S. Miao, S. Xie, F. Yang, Y. Li, G. Wang and X. Bao, Coordinatively unsaturated nickel-nitrogen sites towards selective and high-rate CO2 electroreduction, *Energy Environ. Sci.*, 2018, **11**, 1204–1210.

41   S. Pugliese, N. T. Huan, J. Forte, D. Grammatico, S. Zanna, B. L. Su, Y. Li and M. Fontecave, Functionalization of Carbon Nanotubes with Nickel Cyclam for the Electrochemical Reduction of CO2, *ChemSusChem*, 2020, **13**, 6449–6456.

42   K. Mou, Z. Chen, X. Zhang, M. Jiao, X. Zhang, X. Ge, W. Zhang and L. Liu, Highly Efficient Electroreduction of CO $_2$ on Nickel Single-Atom Catalysts: Atom Trapping and Nitrogen Anchoring, *Small*, 2019, **15**, 1903668.

43   C. Gao, Z. Peng and X. Wu, Controllable synthesis of hollow NiSe2 spheres as an active electrocatalyst for hydrogen evolution reaction, *https://doi.org/10.1142/S1793604720500332*, , DOI:10.1142/S1793604720500332.

44   L. F. Huang, M. J. Hutchison, R. J. Santucci, J. R. Scully and J. M. Rondinelli, Improved Electrochemical Phase Diagrams from Theory and Experiment: The Ni-Water System and Its Complex Compounds, *J. Phys. Chem. C*, 2017, **121**, 9782–9789.

45   J. Masud, W. P. R. Liyanage, X. Cao, A. Saxena and M. Nath, Copper Selenides as High-Efficiency Electrocatalysts for Oxygen Evolution Reaction, *ACS Appl. Energy Mater.*, 2018, **1**, 4075–4083.

46   H. Singh, M. Marley-Hines, S. Chakravarty and M. Nath, Multi-walled carbon nanotube supported Manganese Selenide as Highly Active Bifunctional OER and ORR electrocatalyst, *J. Mater. Chem. A*, 2022, **6**, 4883–5230.

47   R. Shi, J. Guo, X. Zhang, G. I. N. Waterhouse, Z. Han, Y. Zhao, L. Shang, C. Zhou, L. Jiang and T. Zhang, Efficient wettability-controlled electroreduction of CO2 to CO at Au/C interfaces, *Nat. Commun. 2020 111*, 2020, **11**, 1–10.